

Journal of Materials Chemistry A

Accepted Manuscript



This is an *Accepted Manuscript*, which has been through the Royal Society of Chemistry peer review process and has been accepted for publication.

Accepted Manuscripts are published online shortly after acceptance, before technical editing, formatting and proof reading. Using this free service, authors can make their results available to the community, in citable form, before we publish the edited article. We will replace this *Accepted Manuscript* with the edited and formatted *Advance Article* as soon as it is available.

You can find more information about *Accepted Manuscripts* in the [Information for Authors](#).

Please note that technical editing may introduce minor changes to the text and/or graphics, which may alter content. The journal's standard [Terms & Conditions](#) and the [Ethical guidelines](#) still apply. In no event shall the Royal Society of Chemistry be held responsible for any errors or omissions in this *Accepted Manuscript* or any consequences arising from the use of any information it contains.

Ultrathin Nickel-Iron Layered Double Hydroxide Nanosheets Intercalated with Molybdate Anions for Electrocatalytic Water Oxidation

Na Han, Feipeng Zhao, Yanguang Li*

Institute of Functional Nano & Soft Materials, Soochow University, Suzhou 215123, China

E-mail: yanguang@suda.edu.cn

ABSTRACT:

There have been growing efforts to search for active, robust and cost-effective electrocatalysts for oxygen evolution reaction (OER). Among different candidates, Ni-Fe layered double hydroxide (LDH) holds a great promise for its high activity closely approaching or even outperforming that of the precious metal benchmark in alkaline media. Here, we show that its activity can be further promoted when forming ultrathin LDH nanosheets intercalated with molybdate ions via an exfoliation-free hydrothermal method. In 1 M KOH, these nanosheets exhibit about 3-fold larger OER current density than regular NiFe LDH nanosheets, which was believed to be mostly contributed by their higher available density of electrochemically active sites associated with the ultrathin thickness. The great activity is also accompanied by remarkable durability at different current density levels. At last, we demonstrate that these ultrathin nanosheets can also be directly grown on Ni foam for achieving significant current densities.

Introduction

The direct conversions of solar energy to hydrogen or hydrocarbons through water photolysis or CO₂ reduction represent one of the major options humankind has to meet the ever increasing demand for energy.¹⁻² As the common anodic half-reaction in these important processes, water oxidation or oxygen evolution reaction (OER) holds the decisive key to their success. OER involves multi-step proton-coupled electron transfer, and is kinetically sluggish.¹⁻² It usually demands the assistance of electrocatalysts to lower the overpotential and improve the reaction rate and efficiency. Over the past several decades, people have made considerable efforts searching for efficient, robust and earth-abundant OER electrocatalysts. Of particular interest are those based on first-row transition metals such as Fe, Co, Ni and Mn.¹⁻¹⁰

More than 20 years ago, it was serendipitously discovered from battery research that introducing a small amount of iron impurity to nickel oxide/hydroxide electrodes dramatically enhanced their OER activity.¹¹⁻¹² Even though a detailed understanding of the promoting effect of the impurity is still missing, iron-doped nickel hydroxide/oxide has been established as one of the most active electrocatalysts with activity closely approaching or even outperforming those of the precious metal benchmarks (*i.e.* IrO_x or RuO_x) in alkaline media.^{9-10,13-17} In particular, iron-doped nickel hydroxide in the form of layered double hydroxide (LDH) has drawn special attention.¹⁰ LDH is a family of two dimensional layered materials built from the alternate arrangement of brucite-like cationic layers and charge-balancing anions in the interlayer region.¹⁸ Its large interlayer distance may afford remarkable electrochemically accessible surface areas and great electrocatalytic performance. We showed that the OER activity of NiFe-LDH could be further improved through its covalent coupling with conductive multiwalled carbon nanotubes.¹³ Recently, Hu and colleagues

made considerable progress by liquid phase exfoliation of bulk NiFe-LDH to form monolayered nanosheets.¹⁹ With most of the surface active sites exposed, these monolayered nanosheets present an ideal and unique catalytic platform for OER electrocatalysis. Nevertheless, one main pitfall of the liquid phase exfoliation method is its sophistication, *e.g.* it generally requires continuous processing under an inert atmosphere for more than 2 days.¹⁹⁻²⁰ This limitation prompts us to search for other simple yet effective, exfoliation-free approach to prepare monolayered or few-layered NiFe-LDH nanosheets with optimal electrocatalytic power. In this study, we showed that the incorporation of molybdate ions as the charge-balancing species within interlayers resulted in the formation of ultrathin NiFe-LDH nanosheets, mostly monolayered or few-layered. Compared to regular NiFe-LDH, these ultrathin nanosheets possess over four times higher density of electrochemically active sites, and exhibit about three times larger OER current density.

Experimental Section

Synthesis of ultrathin NiFeMo nanosheets. In a typical synthesis, 0.45 mmol of NiAc₂, 0.05 mmol Fe(NO₃)₃ and 0.1 g of (NH₄)₆Mo₇O₂₄·4H₂O were first dissolved in 10 ml of distilled water. Then, 0.12 g of urea was added to the above solution, and stirred for 30 min. The resulting solution was transferred to a 20 ml Teflon-lined autoclave, and hydrothermally treated at 160 °C for 2-10 h. Final products were collected by centrifugation, repetitively washed and vacuum-dried.

Material characterizations: X-ray diffraction (XRD) was performed on PANalytical X-ray diffractometer at a scan rate of 0.05°/s. Scanning electron microscopy (SEM) images were taken from Zeiss scanning electron microscope. Transmission electron microscopy (TEM) was conducted on FEI Tecnai F20 transmission electron microscope at an acceleration voltage of 200 kV. X-ray

photoelectron spectra (XPS) were collected on an SSI S-Probe XPS Spectrometer. Raman spectra were collected from Renishaw inVia plus Raman microscope with 514 nm wavelength laser excitation under 1 mW power.

Electrochemical Measurements. 1 mg of catalyst, 0.5 mg of Ketjen black and 5 μl of 5 wt% Nafion solution were dispersed in 0.25 ml of 1:1 v/v water/ethanol with the assistance of at least 30 min sonication to form a homogeneous ink. For measurements on regular glassy carbon electrode, 5 μl of the catalyst ink was loaded onto the working electrode of 3 mm in diameter (loading 0.28 mg/cm^2). For measurements on glassy carbon rotating disk electrode, 14 μl of the catalyst ink was loaded onto the working electrode of 5 mm in diameter (loading 0.28 mg/cm^2). For measurements on carbon fiber paper, 70 μl of the catalyst ink was loaded onto the working electrode of $1 \times 1 \text{ cm}^2$ (loading 0.28 mg/cm^2).

Electrochemical measurements were carried out in 1 M KOH within a standard three electrode system controlled by a CHI 660E potentiostat. Graphite rod was used as the counter electrode and saturated calomel electrode as the reference electrode. Prior to data collection, the electrocatalyst was cycled until a stable curve was developed. Cyclic voltammetry (CV) data was collected at 10 mV/s. Chronopotentiometry data were collected under a constant current density specified in the paper on RDE, carbon fiber paper or Ni foam electrode. Experiments involving RDE were conducted with the working electrode continuously rotating at 1600 rpm to get rid of the oxygen bubbles.

Results and Discussion

Intercalation of molybdate ions has been previously demonstrated for some LDHs including MgAl-LDH and ZnAl-LDH by co-precipitation or ion-exchange method, but never studied for

NiFe-LDH.²¹⁻²³ Here, we prepared ultrathin nanosheets of molybdate-intercalated NiFe-LDH (hereafter denoted NiFeMo) using a facile hydrothermal method (see Experimental Details). During the reaction, Ni²⁺ and Fe³⁺ with a molar ratio of 9 were hydrolyzed upon the gradual thermal decomposition of urea in the presence of molybdate salt. Negatively charged molybdate ions were believed to be readily trapped within the gallery of resulting LDH (Figure 1a). Due to the alkaline synthetic environment, they do not polymerize and exist as MoO₄²⁻.²² The nominal formula of NiFeMo was determined to be Ni^(II,III)_{0.9}Fe^(III)_{0.1}(OH)₂(MoO₄)_{0.33}(H₂O)_x based on inductively coupled plasma (ICP) analysis over multiple samples.

We first interrogated the structure of NiFeMo through x-ray diffraction (XRD). LDHs have analogous structures to brucite but with enlarged interlayer distance.¹⁸ Compared to the latter, regular LDHs usually feature intense (00 l) diffraction peaks owing to their high periodicity and preferential crystallographic orientation along the c -direction, whereas other diffraction peaks are much diminished. Such a difference is best illustrated by comparing the XRD patterns of regular NiFe-LDH and brucite β -Ni(OH)₂ prepared via procedures described in our previous reports (Figure 1b).^{13,24} In stark contrast, NiFeMo exhibits pronounced (100) and (110) diffraction peaks in the same position as those of β -Ni(OH)₂ (Figure 1b). Its (00 l) set of diffraction peaks are largely suppressed but still discernible, strongly evidencing the lower periodicity in the direction normal to layers. This is the first indication of the formation of ultrathin nanosheets. To demonstrate the intercalation of molybdate ions within these ultrathin nanosheets, Raman spectra were collected between 200 cm⁻¹ to 1000 cm⁻¹ as shown in Figure 1c. Both NiFeMo and NiFe-LDH exhibit bands at 456 cm⁻¹ and 523 cm⁻¹, which are assignable to the stretching vibration of Ni-OH in LDH materials.¹⁶ In addition, there are several featured modes of MoO₄²⁻ in the Raman spectrum of NiFeMo. These modes are observed

at 319 cm^{-1} , 345 cm^{-1} (bending modes), 854 cm^{-1} (antisymmetric stretching mode), 914 cm^{-1} , 938 cm^{-1} (symmetric stretching modes).²² All of them unambiguously suggest that ultrathin LDH nanosheets in our study are intercalated with MoO_4^{2-} .

We further carried out electron microscopic and spectroscopic characterizations to study the morphology and microstructure of NiFeMo nanosheets. Under scanning electron microscopy (SEM), these nanosheets appear as dark colloidal flakes with a texture resembling that of dried graphene oxide (Figure 2a). Transmission electron microscopy (TEM) examination unveils that NiFeMo nanosheets have a lateral dimension about several hundred nanometers. They are mostly less than three atomic layers thick, with a considerable fraction of monolayers identified. For example, Figure 2b shows such a monolayered nanosheet with clean edges and uniform contrast over the entire nanosheet. Its ultrathin thickness is almost transparent to electron beam inasmuch the lacy carbon back support can be clearly captured through the nanosheet. Figure 2c shows a few-layered nanosheet. From its curved-up edges, we estimate that the thickness is 2~3 atomic layers, and the interlayer distance is $\sim 0.7\text{ nm}$. It is worth noting that this interlayer distance is close to that of molybdate intercalated MgAl-LDH (hydrotalcite).²²⁻²³ Unfortunately, since these ultrathin nanosheets are highly susceptible to thermal damage under strong electron beam radiation, we had difficulty in performing detailed high-resolution TEM imaging. Selected area electron diffraction (SAED) pattern of NiFeMo nanosheet reveals a set of diffraction spots with six-fold symmetry (insert of Figure 2b). It reflects the brucite-like hexagonal arrangement of edge-sharing MO_6 octahedra within each layers. Large-area energy dispersive spectrum (EDS) analysis confirms the presence of Ni, Fe, Mo and O (Figure 2d). Furthermore, to corroborate their ultrathin thickness, NiFeMo nanosheets were dispersed on a silicon wafer for atomic force microscopy (AFM) examination. The typical AFM image was

depicted in Figure 2e. Its corresponding height profile shows an average thickness of ~ 0.5 nm, close to the thickness of a monolayered nanosheet. High-resolution x-ray photoelectron spectroscopy (XPS) spectra of Ni and Fe in NiFeMo are consistent with those of regular NiFe-LDH.¹³ XPS spectrum of Mo also agrees with Mo(VI) in molybdate (Supporting Information Figure S1).

The presence of molybdate ions during the synthesis is critical to the formation of LDH nanosheets with monolayered or few-layered thickness. Even though still uncertain about the exact role they play, we hypothesize that these negatively charged species might stabilize individual positively charged LDH nanosheets and make it thermodynamically or kinetically unfavorable for nanosheets to further extend along the c-direction. Control experiments showed that the simple co-precipitation of Ni^{2+} and Fe^{3+} in the absence of molybdate only yielded thicker irregular particles with a mixed LDH and $\beta\text{-Ni}(\text{OH})_2$ phase (Supporting Information Figure S2). However, the introduction of excessive molybdate ($\text{Mo}/(\text{Ni}+\text{Fe}) \geq 2$) was found to result in a new compound having the NiMoO_4 crystal structure and with nanowire or nanobelt morphology.

Electrocatalytic activity of NiFeMo nanosheets for OER was evaluated in alkaline electrolytes. Experiments were conducted in a standard three-electrode system using a carefully calibrated saturated calomel electrode (SCE) as the reference electrode and a graphite rod as the counter electrode. Catalyst powders were blended with conductive carbon black and Nafion polymer binder, and then uniformly cast onto a glassy carbon electrode as the working electrode. Results were benchmarked against the commercial 20 wt% Ir/C catalyst from Premetek Co, and thin NiFe-LDH nanosheets prepared following our previous report (hereafter denoted as NiFe). In 1 M KOH, the cyclic voltammetry (CV) of NiFeMo exhibits a pair of redox waves centered at ~ 0.33 V (vs. SCE), characteristic of the redox chemistry of $\text{Ni}^{\text{II}}/\text{Ni}^{\text{III}}$ under the inductive effect of Fe (Figure 3a).

Electrocatalytic oxygen evolution on NiFeMo commences at ~ 0.40 V, corresponding to a low overpotential (η) of ~ 240 mV. This value is improved by ~ 30 mV compared to both NiFe and the Ir/C benchmark. The overpotentials required to drive an anodic current density of 10 mA/cm^2 are 280 mV, 310 mV and 315 mV for NiFeMo, Ir/C and NiFe, respectively. The measured activity of NiFeMo is among the best single-component OER electrocatalysts, albeit still not as good as some hybrid materials with conductive carbon (Supporting Information Table S1). Electrochemical impedance analysis at $\eta = 320$ mV also suggests NiFeMo has smaller charge transfer impedance than NiFe (Supporting Information Figure S3). Furthermore, we investigated the influence of Fe/Ni ratio on the electrochemical performance of the final products. It was found that 10 at% Fe affords the optimal OER activity (Supporting Information Figure S4). Adding more than 20 at% Fe adversely affects the performance.

To glean the kinetic information of OER electrocatalysis, we performed Tafel analysis of the three electrocatalysts. They were biased at different overpotentials for sufficiently long time. Only the steady-state OER current density free of capacitive contribution was measured and plotted as a function of the overpotential as shown in Figure 3b. Fitting these data points yields linear lines with different slopes in the overpotential range of $0.25\sim 0.30$ V. Interestingly, both NiFeMo and NiFe have a Tafel slope of 40 mV/decade , but steady-state OER current density of the former is ~ 2.7 -fold larger than that of the latter. The same Tafel slope suggest that the two electrocatalysts share the same rate-determining step and hence a similar electrocatalytic nature for OER. The value is also in a good agreement with the reported number for monolayered NiFe-LDH nanosheets from liquid phase exfoliation,¹⁹ and is smaller than that of Ir/C (55 mV/decade). It has to be added that the Tafel slope for Ir/C measured here may be overestimated due to its continuous degradation over the course of the

measurement.

Furthermore, we probed the origin of the enhanced OER activity of NiFeMo over NiFe by comparing their density of electrochemically active sites. Even though the exact reaction mechanism of Fe-doped Ni hydroxides or oxides is still under debate, it has been suggested that Ni species within this type of electrocatalysts function as the active sites, and neighboring Fe species induce partial charge transfer to Ni sites, and activate them for OER electrocatalysis.¹⁶⁻¹⁷ Given that only surface Ni sites directly participate in the reaction, we approximate the number of active sites by the number of redox-active Ni sites from the integration of Ni^{II}/Ni^{III} anodic wave assuming a one-electron transfer process.^{19,25} It is thereby estimated that the density of electrochemically active sites on NiFeMo is about 4.3 times higher than NiFe. This number of increase can be justified if we consider a model in which nanosheets with an average thickness of ~10 atomic layers (for NiFe) were reduced to 1~3 atomic layers (for NiFeMo). We believe that it largely accounts for the 2.7-fold increase in OER current density. Similar effects were also noticed in the study of monolayered NiFe, CoCo and CoMn-LDH nanosheets from liquid phase exfoliation.¹⁹⁻²⁰

A notorious problem plaguing OER electrocatalysts is their insufficient stability. The highly oxidizing environment they are exposed to can cause the degradation of most chemical functional groups. For example, the instability of IrO₂ and RuO₂ in alkaline electrolytes is well documented.²⁶ Despite their popularity among literature, MnO_x as OER electrocatalysts has a large propensity toward further oxidation to soluble Mn^{VII}.²⁷ Our previous investigation also revealed that Co or Fe-based catalysts were subjected to significant morphological change at positive potentials pertinent to OER.²⁸ Relatively speaking, Ni-based catalysts have better electrochemical stability and corrosion resistance. Here, the chronopotentiometry response (V~t) of NiFeMo was collected on different

experimental setups and at several different anodic current densities. Experiments were first carried out at $j = 5 \text{ mA/cm}^2$ on rotating disk electrode with a continuous rotating speed of 1600 rpm to ensure no accumulation of oxygen bubbles on the electrode surface. As shown in Figure 3c, NiFeMo catalyst displays a nearly constant operating potential at $\sim 0.44 \text{ V}$ for over 6000 s. Under the same condition, the Ir/C benchmark starts at $\sim 0.46 \text{ V}$, but undergoes a gradual increase of $\sim 30 \text{ mV}$ during the course of the measurement (Figure 3c). For long-term stability assessment, NiFeMo was loaded on a carbon fiber paper electrode and biased at $j = 5 \text{ mA/cm}^2$, 10 mA/cm^2 and 20 mA/cm^2 , respectively, each for 8 h. As shown in Figure 3d, within each stage, the potential profile remains almost constant in spite of some slight fluctuation. These measurements confirm the good electrochemical stability of NiFeMo under OER conditions.

It is sometimes desirable to directly grow electrode materials on conductive current collectors for electrochemical applications including batteries and electrocatalysis.^{5,29} Direct growth of electrode materials usually improves their electrical and mechanical contact to underneath current collector, and at the same time eliminates the need of polymeric binding additives which commonly introduce additional resistance. Here, we demonstrate that the facile hydrothermal synthesis is also amenable to the direct growth of ultrathin NiFeMo nanosheets on current collectors such as Ni foam. Compared to planar glassy carbon electrode, Ni foam offers a three-dimensional porous framework with superior electric conductivity and large accessible surface areas. As a result, using Ni foam as the current collector usually permits a much higher catalyst loading as well as reduced ohmic drop within the current collector or at the current collector/electrocatalyst interface. Figure 4a shows the photos of NiFeMo on Ni foam electrode. Under SEM, the entire Ni foam framework is revealed to be uniformly coated with ultrathin nanosheets (Figure 4b,c). They have ripples, folds and wrinkles,

again reminiscent of the common surface morphology of graphene nanosheets.

The CV curve of NiFeMo nanosheet-coated Ni foam displays features similar to that collected on glassy carbon electrode except for larger redox waves and OER current density (Figure 4e). It delivers a remarkable anodic current density of 100 mA/cm² at 0.46 V and 200 mA/cm² at 0.48 V. The high electrocatalytic performance is mainly contributed by NiFeMo inasmuch bare Ni foam has negligible OER activity under the investigated potential range. We likewise evaluated the durability of nanosheet-coated Ni foam electrode. As shown in Figure 4f, during the course of successive biasing under large anodic current density of $j = 20$ mA/cm² and then 50 mA/cm² each for 10 h, the electrode presents an initial activation followed by stable potentiometric response. Furthermore, we examined the surface morphology of nanosheet-coated Ni foam electrode at the end of 20 h durability test (Figure 4d). It is apparent that NiFeMo nanosheets on electrode surface become roughened with the formation of rich ridges and cavities. We believe such a morphological change is caused by the surface tension of evolving oxygen bubbles. It stretches or squeezes flexible nanosheets, significantly modifying their surface morphology. However, we do not observe any significant film rupture over the entire electrode. This corroborates the robustness of nanosheet-coated Ni foam electrode even under large operation current densities with vigorous evolution of oxygen bubbles.

Conclusions

In summary, we prepared ultrathin nanosheets of molybdate intercalated NiFe-LDH by an exfoliation-free hydrothermal method, and demonstrated them as highly efficient and durable electrocatalysts for oxygen evolution reaction in alkaline media. NiFeMo nanosheets only need an overpotential of ~280 mV to drive 10 mA/cm², comparing favorably to the Ir/C benchmark and

regular NiFe nanosheets. Their improved electrocatalytic performance is believed to result from the higher available density of electrochemically active sites associated with the ultrathin thickness. Moreover, we showed that the synthetic method could also be applied to the direct growth of NiFeMo nanosheets on Ni foam, giving rise to working electrodes capable of delivering significant current density with remarkable robustness.

Acknowledgements

We acknowledge supports from the National Natural Science Foundation of China (51472173), the Natural Science Foundation of Jiangsu Province (BK20140302), Jiangsu Key Laboratory for Carbon-Based Functional Materials and Devices, the Priority Academic Program Development of Jiangsu Higher Education Institutions and Collaborative Innovation Center of Suzhou Nano Science and Technology.

Reference

- (1) M. G. Walter, E. L. Warren, J. R. McKone, S. W. Boettcher, Q. Mi, E. A. Santori and N. S. Lewis, *Chem. Rev.*, 2010, **110**, 6446-6473.
- (2) T. R. Cook, D. K. Dogutan, S. Y. Reece, Y. Surendranath, T. S. Teets and D. G. Nocera, *Chem. Rev.*, 2010, **110**, 6474-6502.
- (3) M. W. Kanan and D. G. Nocera, *Science.*, 2008, **321**, 1072-1075.
- (4) Y. Gorlin and T. F. Jaramillo, *J. Am. Chem. Soc.*, 2010, **132**, 13612-13614.
- (5) Y. Li, P. Hasin and Y. Wu, *Adv. Mater.*, 2010, **22**, 1926-1929.
- (6) J. Suntivich, K. J. May, H. A. Gasteiger, J. B. Goodenough and Y. Shao-Horn, *Science.*, 2011, **334**, 1383-1385.
- (7) Y. Liang, Y. Li, H. Wang, J. Zhou, J. Wang, T. Regier and H. Dai, *Nat. Mater.*, 2011, **10**, 780-786.
- (8) R. D. L. Smith, M. S. Prevot, R. D. Fagan, Z. Zhang, P. A. Sedach, M. K. J. Siu, S. Trudel and C. P. Berlinguette, *Science.*, 2013, **340**, 60-63.
- (9) C. C. L. McCrory, S. Jung, J. C. Peters and T. F. Jaramillo, *J. Am. Chem. Soc.*, 2013, **135**, 16977-16987.
- (10) M. Gong and H. Dai, *Nano Res.*, 2015, **8**, 23-39.
- (11) D. A. Corrigan, *J. Electrochem. Soc.*, 1987, **134**, 377-384.
- (12) D. A. Corrigan and R. M. Bendert, *J. Electrochem. Soc.*, 1989, **136**, 723-728.
- (13) M. Gong, Y. Li, H. Wang, Y. Liang, J. Z. Wu, J. Zhou, J. Wang, T. Regier, F. Wei and H. Dai, *J. Am. Chem. Soc.*, 2013, **135**, 8452-8455.

- (14) M. D. Merrill and R. C. Dougherty, *J. Phys. Chem. C*, 2008, **112**, 3655-3666.
- (15) L. Trotochaud, J. K. Ranney, K. N. Williams and S. W. Boettcher, *J. Am. Chem. Soc.*, 2012, **134**, 17253-17261.
- (16) M. W. Louie and A. T. Bell, *J. Am. Chem. Soc.*, 2013, **135**, 12329-12337.
- (17) L. Trotochaud, L. Young Samantha, K. Ranney James and W. Boettcher Shannon, *J Am Chem Soc*, 2014, **136**, 6744-6753.
- (18) Q. Wang and D. O'Hare, *Chem. Rev.*, 2012, **112**, 4124-4155.
- (19) F. Song and X. Hu, *Nat. Commun.*, 2014, **5**, 4477.
- (20) F. Song and X. Hu, *J. Am. Chem. Soc.*, 2014, **136**, 16481-16484.
- (21) X. Yu, J. Wang, M. Zhang, P. Yang, L. Yang, D. Cao and J. Li, *Solid State Sci.*, 2009, **11**, 376-381.
- (22) R. L. Frost, A. W. Musumeci, W. N. Martens, M. O. Adebajo and J. Bouzaid, *J. Raman Spectrosc.*, 2005, **36**, 925-931.
- (23) R. Zavoianu, R. Birjega, O. D. Pavel, A. Cruceanu and M. Alifanti, *Appl. Catal. A*, 2005, **286**, 211-220.
- (24) Y. Li, B. Tan and Y. Wu, *Chem. Mater.*, 2007, **20**, 567-576.
- (25) M. Gao, W. Sheng, Z. Zhuang, Q. Fang, S. Gu, J. Jiang and Y. Yan, *J. Am. Chem. Soc.*, **2014**, **136**, 7077-7084.
- (26) K. Kinoshita *Electrochemical Oxygen Technology*, 1992.
- (27) Y. Li and H. Dai, *Chem. Soc. Rev.*, 2014, **43**, 5257-5275.
- (28) Y. Li, M. Gong, Y. Liang, J. Feng, J.-E. Kim, H. Wang, G. Hong, B. Zhang and H. Dai, *Nat. Commun.*, 2013, **4**, ncomms2812, 2817 pp.
- (29) Y. Li, B. Tan and Y. Wu, *Nano Lett.*, 2008, **8**, 265-270.

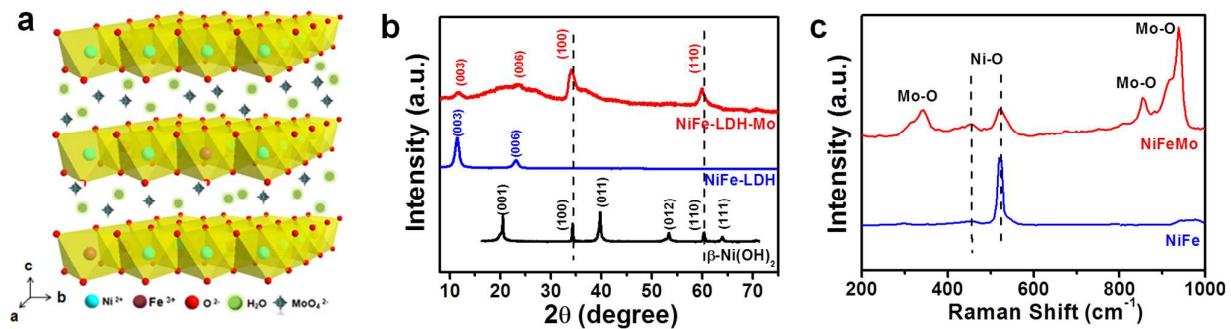


Figure 1. (a) Schematic crystal structure of NiFeMo. (b) XRD patterns of NiFeMo along with NiFe and β -Ni(OH)₂ for comparison, the suppressed (00*l*) peaks for NiFeMo are indicative of ultrathin nanosheet thickness. (c) Raman spectra of NiFeMo and NiFe showing the fingerprint vibrations of Ni-OH and MoO₄²⁻.

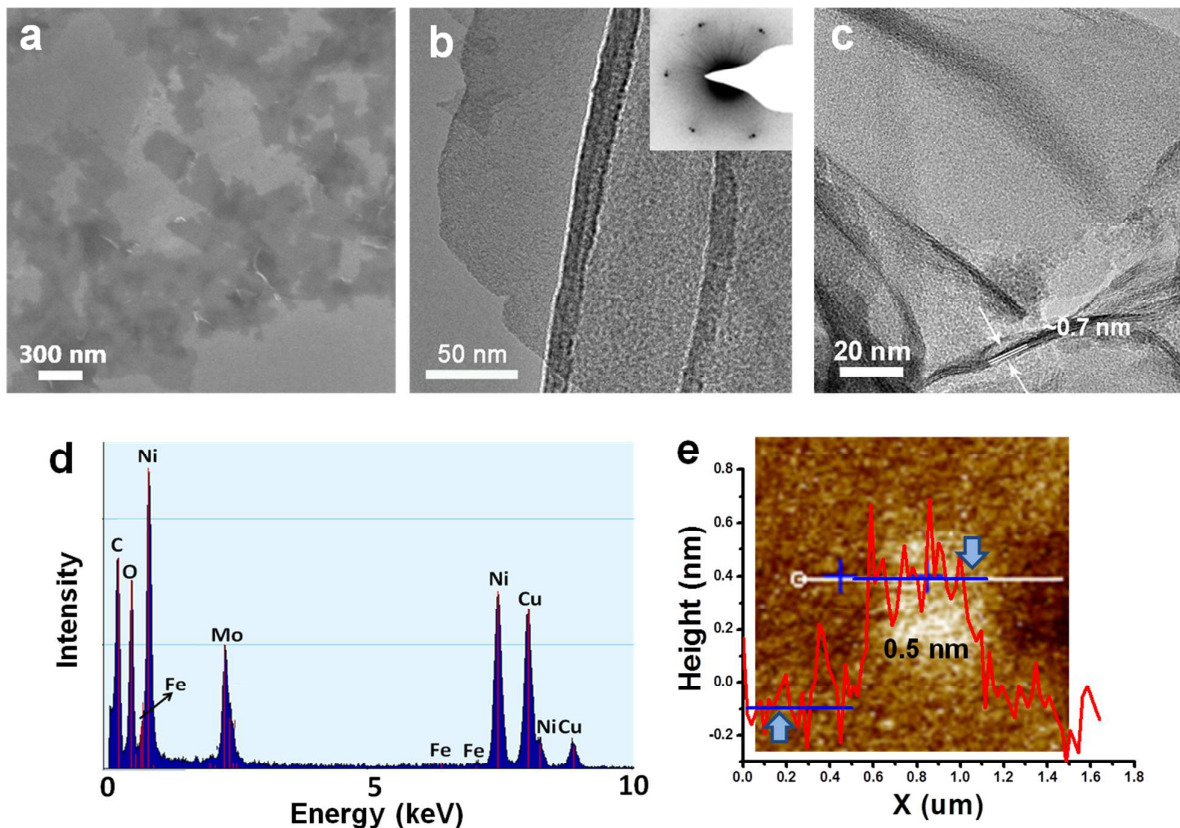


Figure 2. Microscopic characterizations of ultrathin NiFeMo nanosheets. (a) SEM image, (b-c) TEM images with corresponding SEAD pattern shown as the insert of (b), (d) large-area EDS analysis, and (e) AFM image with associated height profile.

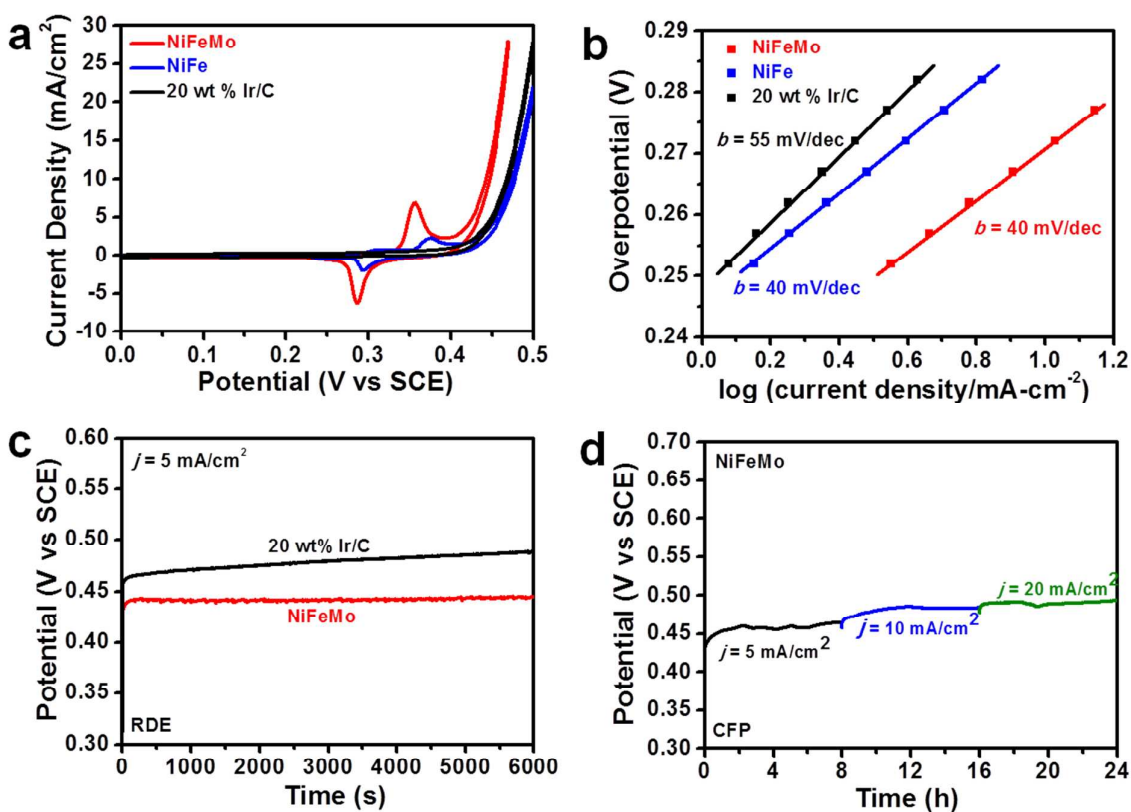


Figure 3. Electrochemical measurements of NiFeMo nanosheets for OER electrocatalysis. (a) CV curve of NiFeMo along with NiFe and 20 wt% Ir/C for comparison. (b) Their corresponding steady-state current densities at several overpotentials fit by the Tafel equation. (c) Chronopotentiometry response ($V \sim t$) of NiFeMo and Ir/C electrocatalysts when loaded on rotating disk electrode. (d) Chronopotentiometry response of NiFeMo at different current densities when loaded on carbon fiber paper. The electrolyte in use is 1 M KOH.

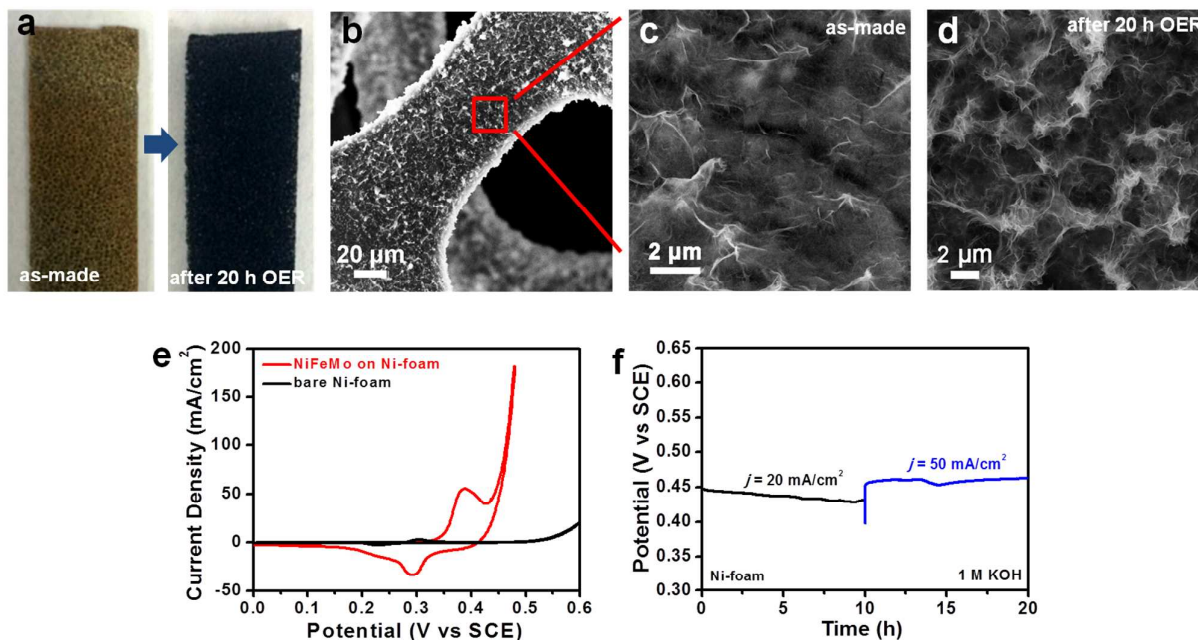
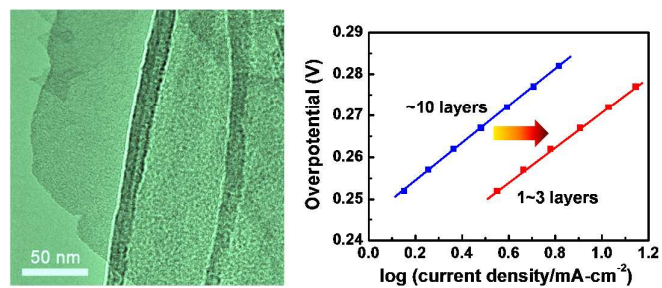


Figure 4. Electrocatalytic performance of Ni foam electrodes covered with directly grown NiFeMo nanosheets (NiFeMo/Ni). (a) Photos of as-made and aged NiFeMo/Ni electrode. (b-c) SEM images of as-made NiFeMo/Ni electrode. (d) SEM image of used NiFeMo/Ni electrode after extensive durability measurement. (e) CV curves of NiFeMo/Ni electrode and bare Ni foam electrode. (f) Chronopotentiometry response of NiFeMo/Ni at $j = 20 \text{ mA/cm}^2$ and 50 mA/cm^2 .

TOC



Incorporation of molybdate ions in NiFe-LDH structure leads to the formation of ultrathin nanosheets with enhanced OER performance.